ChemBioChem

Combining Chemistry and Biology

Chemistry Europe

European Chemical Societies Publishing

Accepted Article

Title: Human 2´-Deoxynucleoside 5´-Phosphate N-Hydrolase 1: The Catalytic Roles of Tyr24 and Asp80

Authors: Anna E. Carberry, Suneeta Devi, David J. Harrison, and Rafael G. da Silva

To be cited as: *ChemBioChem* **2024**, e202400047

Link to VoR: https://doi.org/10.1002/cbic.202400047

WILEY VCH

WILEY VCH

RESEARCH ARTICLE

Human 2′-Deoxynucleoside 5′-Phosphate *N*-Hydrolase 1: The Catalytic Roles of Tyr24 and Asp80

Anna E. Carberry,[a] Suneeta Devi,[a] David J. Harrison,[b,c] and Rafael G. da Silva*[a]

[a] A. E. Carberry, S. Devi, R. G. da Silva
School of Biology, Biomedical Sciences Research Complex
University of St Andrews
St Andrew, KY16 9ST, United Kingdom
E-mail: rgds@st-andrews.ac.uk

[b] D. J. Harrison
School of Medicine,
University of St Andrews
St Andrew, KY16 9TF, United Kingdom

[c] D. J. Harrison
NuCana Plc
Edinburgh, EH12 9DT, United Kingdom

Supporting information for this article is given via a link at the end of the document.

Abstract: The human enzyme 2′-deoxynucleoside 5′-phosphate *N*-hydrolase 1 (*Hs*DNPH1) catalyses the hydrolysis of 5-hydroxymethyl-2′-deoxyuridine 5′-phosphate to generate 5-hydroxymethyluracil and 2-deoxyribose-5-phosphate via a covalent 5-phospho-2-deoxyribosylated enzyme intermediate. *Hs*DNPH1 is a promising target for inhibitor development towards anticancer drugs. Here, site-directed mutagenesis of conserved active-site residues, followed by HPLC analysis of the reaction and steady-state kinetics are employed to reveal the importance of each of these residues in catalysis, and the reaction pH-dependence is perturbed by each mutation. Solvent deuterium isotope effects indicate no rate-limiting proton transfers. Crystal structures of D80N-*Hs*DNPH1 in unliganded and substrate-bound states, and of unliganded D80A- and Y24F-*Hs*DNPH1 offer atomic level insights into substrate binding and catalysis. The results reveal a network of hydrogen bonds involving the substrate and the E104-Y24-D80 catalytic triad and are consistent with a proposed mechanism whereby D80 is important for substrate positioning, for helping modulate E104 nucleophilicity, and as the general acid in the first half-reaction. Y24 positions E104 for catalysis and prevents a catalytically disruptive close contact between E104 and D80.

Introduction

The human enzyme 2′-deoxynucleoside 5′-phosphate *N*-hydrolase 1 (*Hs*DNPH1) (EC 3.2.2.-)[1] catalyses the *N*-ribosidic bond cleavage of 5-hydroxymethyl-2′-deoxyuridine 5′-monophosphate (5hmdUMP), a cytotoxic nucleotide resulting from the deamination of epigenetically modified 5-hydroxymethyl-2′-deoxycytidine 5′-monophosphate, to generate 5-hydroxymethyluracil (5hmUra) and 2-deoxyribose 5-phosphate[2] (Scheme 1). The presence of 5hmdUMP in the nucleotide pool and its eventual erroneous incorporation into DNA requires nucleotide excision and repair, usually single-strand break repair by poly(ADP)-ribose polymerase 1 (PARP1). In breast cancer gene (BRCA)-deficient cancers, PARP1 inhibitors (PARPi) trap PARP1 at the 5hmdUMP-induced DNA single-strand repair site, resulting in synthetic lethality because, unlike healthy cells, BRCA$^{-/-}$ cancer cells cannot undergo homologous recombination to repair DNA.[2-3] Accordingly, increased cellular 5hmdUMP concentration enhances sensitivity of *BRCA*-deficient tumours (breast, prostate, pancreatic and ovarian cancers) to PARPi, while upregulation of *Hs*DNPH1 leads to PARPi resistance as the enzyme depletes 5hmdUMP levels.[2] Hence, *Hs*DNPH1 is a promising target for inhibition to potentiate PARPi action and to counter resistance to PARPi therapy resulting from 5hmdUMP depletion.[2]

To help elucidate its catalytic mechanism and aid inhibitor design, *Hs*DNPH1 structures have been solved in unliganded form and bound to the slow-reacting substrate 2′-deoxyuridine 5′-monophosphate (dUMP),[4] and in complex with an inhibitor.[5] *Hs*DNPH1's specificity constant k_{cat}/K_M is 1,940-fold higher for 5hmdUMP than for dUMP at 37 °C.[4, 6] Structural and kinetic studies using dUMP as substrate hypothesized a double-displacement mechanism where the conserved E104 residue would act as a nucleophile to form a covalent 5-phospho-2-deoxyribosyl-enzyme intermediate in the first half-reaction, and the conserved D80 residue would serve as the general base to activate a water molecule to hydrolyse this intermediate in the second half-reaction.[4] Intriguingly, E104 was found *in crystallo* in a strong hydrogen bond (H-bond) with the conserved residue Y24.[4]

Recently, the crystal structures of an E104Q-*Hs*DNPH1 mutant bound to 5hmdUMP, and, crucially, an E55Q-*Hs*DNPH1 mutant covalently bound to the 2-deoxyribosyl-5-phosphate intermediate via E104 were obtained. The latter structure provided direct evidence for the double-displacement mechanism, but showed that E55, not D80, was the general base in the second half-

reaction.[7] The importance of Y24 and D80 to *Hs*DNPH1 catalysis, if any, remained an open question.

Here we describe the biocatalytic synthesis of 5hmdUMP, and its use, along with pH-rate profiles, solvent deuterium isotope effects, site-directed mutagenesis, high-performance liquid chromatography (HPLC), differential scanning fluorescence (DSF), and protein crystallography to characterise the wild-type *Hs*DNPH1 (WT-*Hs*DNPH1) reaction and assess the contributions of Y24, D80, and other conserved residues to catalysis. The findings advance our mechanistic understanding of *Hs*DNPH1 catalysis and may help inform inhibitor design.

Results and Discussion

Production of *Hs*DNPH1 Variants

Full-length *Hs*DNPH1 variants, used for biochemical and biophysical analysis, and N-terminally truncated *Hs*DNPH1 variants, used for crystallography,[4] were purified to homogeneity as estimated by Coomassie Blue-stained SDS-PAGE (Figure S1). Electrospray ionization-time-of-flight mass spectrometry (ESI-TOF-MS) confirmed the expected masses of all variants (Figure S2).

Biocatalytic Production of 5hmdUMP

Chemical synthesis of 2′-deoxynucleotides are often cumbersome, requiring high temperatures, hazardous chemicals, and several protection and deprotection steps.[8] We developed a one-pot, room temperature, biocatalytic route to 5hmdUMP from commercially available 5hmUra and 2′-deoxyinosine. First, a 2-deoxyribosyl-transfer reaction catalysed by *Bacillus psychrosaccharolyticus* nucleoside 2-deoxyribosyltransferase (*Bp*NDT)[9] was used to form 5-hydroxymethyl-2′-deoxyuridine. Xanthine oxidase was used to drive forward the reaction equilibrium by converting the hypoxanthine coproduct to uric acid. Selective phosphorylation of the 5-hydroxymethyl-2′-deoxyuridine to yield 5hmdUMP was achieved by adding *Drosophila melanogaster* 2′-deoxynucleoside kinase[10], ATP, and $MgCl_2$, along with pyruvate kinase and phosphoenolpyruvate to regenerate ATP. The final product was purified by anion exchange, and showed one peak by HPLC (Figure 1a). High-resolution desorption electrospray ionization mass spectrometry (DESI-MS) detected the desired m/z (Figure 1b), and the UV-VIS absorbance spectrum (Figure 1c) showed the characteristic λ_{max} at 264 nm.[11] Both ^{1}H-NMR and ^{31}P-NMR spectra are shown in Figures S3 and S4, respectively.

pH-rate profile of WT-*Hs*DNPH1

To allow a more detailed mechanistic analysis of the *Hs*DNPH1 reaction, we developed a direct and continuous activity assay. We determined the extinction coefficient at 264 nm (ε_{264}) of 5hmUra to be 8000 M^{-1} cm^{-1} (Figure S5), which allowed quantification of substrate consumption during the *Hs*DNPH1-catalysed reaction under steady-state conditions based on a $\Delta\varepsilon_{264}$ of 2,200 M^{-1} cm^{-1} when compared with the ε_{264} of 5hmdUMP (10,200 M^{-1} cm^{-1}).[11] Initial rates were dependent on *Hs*DNPH1 concentration (Figure S6). A 5hmdUMP saturation curve at 37 °C was fitted to equation (1) to yield a steady-state catalytic rate constant (k_{cat}) of 0.34 ± 0.01 s^{-1} (value ± fitting error), in excellent agreement with the k_{cat} recently published using a continuous coupled assay.[6] Owing to the relatively low sensitivity of our assay, the lowest concentration of 5hmdUMP (2.5 μM) that resulted in a reliable rate measurement was only marginally below the Michaelis constant (K_M) of 3.5 ± 0.4 μM; thus, this value should be interpreted with caution, even though it lies within 2-fold of that recently reported.[6]

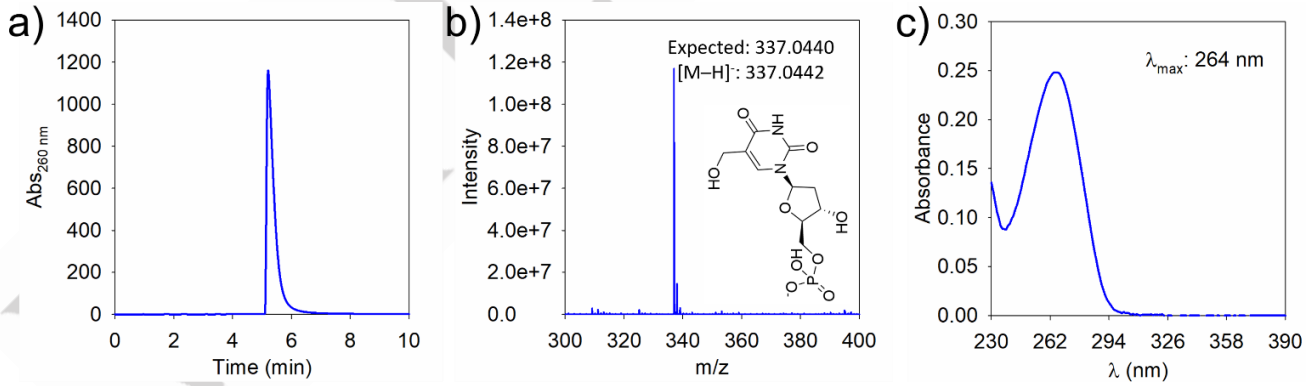

Figure 1. Characterisation of biocatalytically synthesized 5hmdUMP. a) HPLC elution profile of 5hmdUMP. b) High-resolution DESI-MS analysis in negative mode of 5hmdUMP. The inset depicts a possible ionisation state whose expected m/z matches the experimental values. c) UV-VIS spectrum of 5hmdUMP, with a peak at 264 nm.

To permit comparison with recently reported kinetic parameters for WT and mutant *Hs*DNPH1,[7] all subsequent kinetic measurements were carried out at 25 °C. To probe the role of acid-base catalysis in the *Hs*DNPH1 hydrolysis of 5hmdUMP, a pH-rate profile was obtained. Because of the apparently low K_M, only data on k_{cat} was obtained, and fit of the seemingly bell-shaped profile (Figure 2a) to equation (2) showed k_{cat} decreases upon deprotonation of a group with an apparent pK_a of 7.8 ± 0.2. While k_{cat} seems to decrease upon protonation of another group, its predicted pK_a lies below 6.0, the lowest pH employed. The

group that must be deprotonated for maximum catalysis is probably E104, the nucleophile in the covalent catalytic mechanism.[7] Candidates for the group that must be protonated for maximum catalysis include Y24, which shares an H-bond with E104, and D80, which has been hypothesized to donate a proton to the anionic 5hmUra leaving group in the first half-reaction.[4]

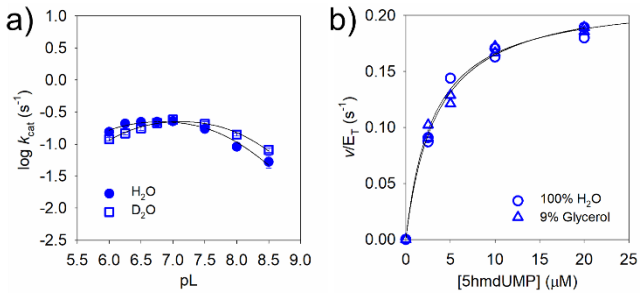

Figure 2. *Hs*DNPH1 kinetics. a) *Hs*DNPH1 pH-k_{cat} and pD-k_{cat} profiles. Data are fitting value ± fitting error of 5hmdUMP saturation curves at different pHs, with two independent measurements at each substrate concentration. The L in pL denotes either H or D. The lines are best fit to equation (2). b) Substrate saturation curves in either 0% or 9% glycerol (v/v). All data points are shown for two independent measurements. The lines represent best fit to equation (1).

The pD-k_{cat} profile showed a displacement to higher pK_as (Figure 2a), with a basic limb pK_a of 8.1 ± 0.1, a common observation due to the increase of ~0.5 units in the pK_as of monoprotic acids in D_2O as compared with the corresponding values in H_2O.[12] Importantly, the pL-independent k_{cat}s produced a solvent deuterium kinetic isotope effect ($^{D2O}k_{cat}$) of 1.0 ± 0.1, indicating that proton transfers do not accompany rate-limiting steps for k_{cat}. At pH 7.0, where *Hs*DNPH1 k_{cat} is highest, substrate saturation curves (Figure 2b) produced a k_{cat} of 0.22 ± 0.01 s^{-1}, and a predicted K_M of 3.1 ± 0.4 μM, although the latter is too close to the lowest nonzero 5hmdUMP concentration used (2.5 μM). Therefore, it is more accurate to interpret 3.1 μM as an upper limit for the *Hs*DNPH1 K_M ($k_{cat}/K_M \geq 7.1 \times 10^4$ M^{-1} s^{-1}). For comparison, an *Hs*DNPH1 K_M of 2.1 μM at 25 °C and pH 7.0 was recently reported.[7] A substrate saturation curve in 9% glycerol (v/v), mimicking the equivalent viscosity of ~100% D_2O at 25 °C, produced no solvent viscosity effect (Table 1), suggesting diffusional steps encompassed by k_{cat} (release of the two reaction products) are kinetically insignificant.[13]

Site-directed mutants of *Hs*DNPH1

To probe the catalytic contribution of several active-site residues, Y24F-, Y24H-, Y24K-, E104A-, E104D-, D80N-, D80A-, R30A-, and H56A-*Hs*DNPH1 variants were characterised. Reaction mixtures containing, in turn, 5hmdUMP (150 μM) and each of the *Hs*DNPH1 variants (20 μM) were analysed by HPLC after being allowed to react for 6 h at 25 °C (Figure 3a and Figure S8). The reactions catalysed by Y24F-, D80N-, D80A-, R30A-, and H56A-*Hs*DNPH1, as well as WT-*Hs*DNPH1, went to completion, showing these variants are active and capable of multiple turnovers. On the other hand, E104A-*Hs*DNPH1 was inactive, as expected given the absence of the nucleophilic residue, as reported for an E104Q-*Hs*DNPH1 variant,[7] but so was Y24K-*Hs*DNPH1, indicating a linear chain with positive charge disrupts the charge balance and/or positioning, required for catalysis, around E104. Curiously, variants E104D-*Hs*DNPH1 and Y24H-*Hs*DNPH1 displayed incomplete conversion, as peaks matching the retention time of 5hmdUMP and 5hmUra remained after 6 h. It is possible that either the activity of these variants is extremely reduced and they would take much longer than 6 h to reach reaction completion, they are capable of only one turnover (or half-turnover), or they are unstable and unfolded before the reaction reached completion.

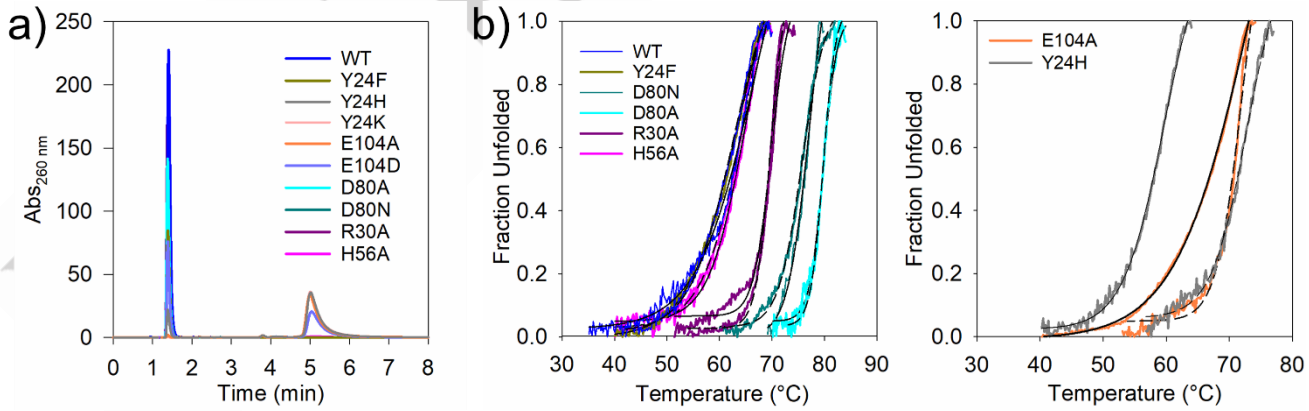

Figure 3. Characterisation of *Hs*DNPH1 variants. a) HPLC elution profiles of the reaction catalysed by *Hs*DNPH1 variants. The substrate 5hmdUMP elutes at ~4.9 min, whereas the product 5hmUra elutes at ~1.4 min. b) DSF-based thermal denaturation of *Hs*DNPH1 variants in the absence and presence of 5hmdUMP. Black lines (solid lines: in the absence of 5hmdUMP; dashed lines: in the presence of 5hmdUMP) are best fit to equation (3).

DSF-based thermal denaturation assays (Figure 3b and Table S1) showed D80N-, D80A-, and E104A-*Hs*DNPH1 have increased melting temperatures (T_m) relative to WT-*Hs*DNPH1, and the presence of 5hmdUMP had no significant effect on their T_m. Y24H-*Hs*DNPH1 T_m drastically increased (ΔT_m = +13 °C) in the presence of 5hmdUMP. E104D- and Y24K-*Hs*DNPH1 did not

produced interpretable DSF data, as they seemed significantly unfolded even at the lowest temperature.

pH-rate profiles of *Hs*DNPH1 mutants

Given that Y24F-, D80N-, D80A-, R30A-, and H56A-*Hs*DNPH1 were capable of multiple catalytic turnovers, their steady-state kinetics were evaluated over different pHs (Figure 4a) to gauge the contribution of residues Y24, D80, H56, and R30 to *Hs*DNPH1 catalysis. Y24F-*Hs*DNPH1 produced a similar pH-k_{cat} profile to WT-*Hs*DNPH1, with a group with apparent pK_a below 6.0 required to be deprotonated for maximum catalysis, and another with apparent pK_a of 8.1 ± 0.1 that must be protonated for maximum catalysis. This suggests that Y24 is unlikely to be the group whose protonation state is reflected in the basic limb of WT-*Hs*DNPH1 pH-k_{cat} profile, but its absence probably causes a small increase in the pK_a of that group from 7.8 to 8.1. Furthermore, Y24F-*Hs*DNPH1 k_{cat} is reduced 400-fold as compared with WT-*Hs*DNPH1, indicating Y24 contributes ~3.6 kcal/mol to *Hs*DNPH1 catalysis, based on equation (4).

The D80N-*Hs*DNPH1 pH-k_{cat} profile only showed a decrease in the acidic limb, upon protonation of a group with an apparent pK_a of 6.1 ± 0.2. Although the value must be taken with caution as it is within experimental error of the lowest pH value employed, this pK_a likely reflects the ionisation state of E104, as in the WT- and Y24F-*Hs*DNPH1 profiles. Interestingly, the basic limb of the D80N-*Hs*DNPH1 profile was flattened, suggestive that the group whose deprotonation abolishes catalysis in the WT enzyme is either D80 or directly influenced by its protonation state. This notion is reinforced by the D80A-*Hs*DNPH1 pH-k_{cat} profile, which is pH-independent, and also points to the loss of H-bond donor/acceptor ability upon the D80A substitution as perturbing the pK_a of E104. The D80N and D80A substitutions result in 129- and 629-fold lower k_{cat} relative to the WT variant (Table 1), consistent with D80 contributing ~2.9 kcal/mol to catalysis from its ability to participate in acid-base chemistry (which is lost in D80N-*Hs*DNPH1), and another ~1.0 kcal/mol from its capacity to participate in H-bonds (which is further lost in D80A-*Hs*DNPH1).

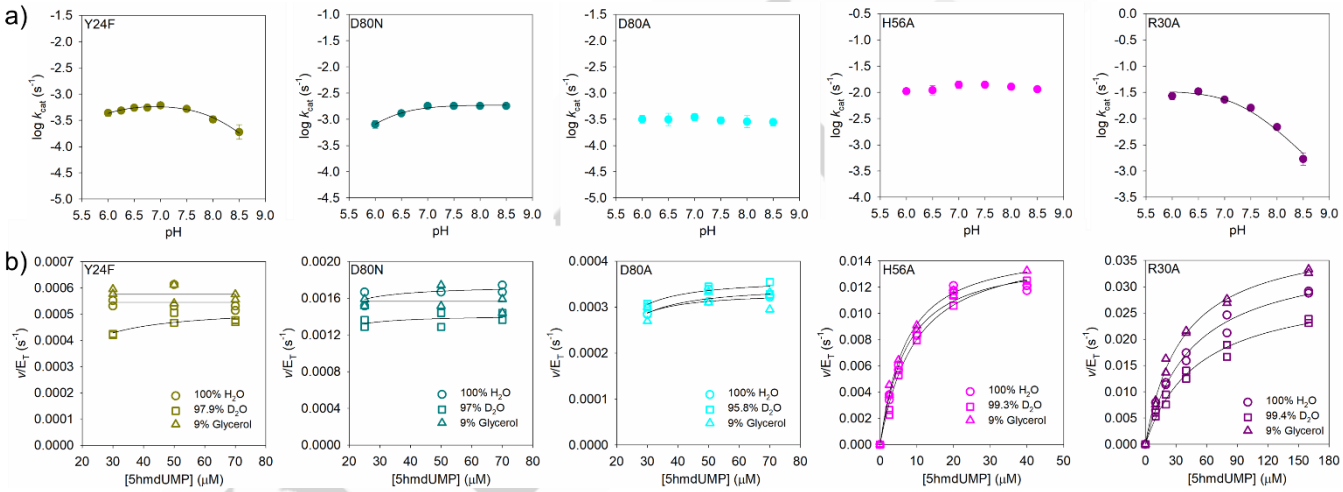

Figure 4. Enzyme kinetics of *Hs*DNPH1 mutants. a) pH-kcat profiles of active-site *Hs*DNPH1 variants. Data are fitting value ± fitting error of 5hmdUMP saturation curves at different pHs, with two independent measurements at each substrate concentration. The lines are best fit to either equation (2) for Y24F, equation (5) for D80N, or equation (6) for R30A. b) Substrate saturation curves in either H_2O, D_2O, or glycerol. All data points are shown for two independent measurements. The lines represent best fit to either equation (1) for R30A or equation (7) for H56A, Y24F, D80N, and D80A.

In the recently reported crystal structure of E104Q-*Hs*DNPH1, H56 donated an H-bond to O2 of 5hmdUMP, and an H56A mutation decreased activity 11-fold relative to WT-*Hs*DNPH1.[7] In agreement, our results showed H56A-*Hs*DNPH1 has a 15-fold lower k_{cat} in comparison to WT-*Hs*DNPH1 (Table 1), a relatively modest catalytic contribution (~1.6 kcal/mol) when compared to those of Y24 and D80. However, this value was pH-independent, demonstrating the H56's ability to participate in polar interactions and/or acid-base chemistry influences the pK_a of key groups in the active site. H56A-*Hs*DNPH1 k_{cat}/K_M of 2.5 × 10^3 M^{-1} s^{-1} is ~28-fold lower than the WT value, pointing to a slightly higher contribution of H56 to the first half-reaction, which ends upon departure of 5hmdUra from the 5-phospho-2-deoxyribosylated enzyme, in agreement with a previous suggestion.[7]

R30A-*Hs*DNPH1 led to just an ~6-fold decrease in k_{cat} as compared with WT-*Hs*DNPH1 (Table 1), in excellent agreement

with recently published observations.[7] R30 interacts with the O4 of 5hmUra moiety of 5hmdUMP via a water molecule.[7] Interestingly, R30A-*Hs*DNPH1 K_M increased to 46 ± 5 μM (Figure 4b), which resulted in a k_{cat}/K_M of 804 M^{-1} s^{-1}, at least an 88-fold reduction from the WT value. This indicates that R30 makes a more sizable contribution to the first half-reaction. Moreover, the R30A-*Hs*DNPH1 k_{cat}/K_M with dUMP as a substrate (5 M^{-1} s^{-1}) is reduced only ~3-fold from the WT-*Hs*DNPH1 k_{cat}/K_M with dUMP (16 M^{-1} s^{-1}) (Figure S9), showing R30's contribution to k_{cat}/K_M is only relevant with the physiological substrate. Intriguingly, the R30A substitution shifted the optimum pH for k_{cat} from 7.0 to 6.5 (Figure 4a), with k_{cat} decreasing upon deprotonation of a group with an apparent pK_a of 7.3 ± 0.3. This suggests R30, and/or its interaction with another group, helps modulate the pK_a of another active-site group, since it is unlikely that R30 itself participates in acid-base chemistry.

Interestingly, the $^{D2O}k_{cat}$ for all *Hs*DNPH1 variants were either unity or near unity (Figure 4B and Table 1). This indicates that even for variants with a significantly decreased k_{cat}, including those where a residue suspected to be directly involved in acid-base chemistry is absent (such as D80N and D80A), proton transfers do not occur in a rate-limiting step. On one hand, if *N*-ribosidic bond cleavage were rate-limiting for the first half-reaction or the overall reaction, protonation of the anionic leaving group can be envisioned to be fast, since it likely happens after the C1′–N1 bond breaking transition state based on other pyrimidine nucleoside *N*-ribosidic bond-cleaving enzymes.[14] On the other hand, if nucleophilic attack by a water molecule were rate-limiting for the second half-reaction or the overall reaction, it would be more difficult to envision proton abstraction by E55 and nucleophilic water activation not occurring in the same transition state as the C1–O bond formation, which would produce a sizable $^{D2O}k_{cat}$.

Crystal structures of D80N-, D80A-, and Y24F-*Hs*DNPH1

To gain further insight into the role of the Y24 and D80 in catalysis, the crystal structure of D80N-*Hs*DNPH1 was solved in complex with 5hmdUMP, and D80A-*Hs*DNPH1 and Y24F-*Hs*DNPH1 structures were solved in their unliganded forms, with data to 1.75-, 1.95-, 2.14-Å resolution, respectively. Data processing and refinement statistics are summarised in Table S2. D80N-*Hs*DNPH1 crystallised with a dimer and one subunit of another dimer in the asymmetric unit. Interestingly, only one of the subunits of the full dimer and the subunit of the other dimer showed electron density for 5hmdUMP in the active site (Figure 5a and Figure S10), whereas the other subunit of the fully formed dimer was in its unliganded state (Figure 5b).

In the D80N-*Hs*DNPH1:5hmdUMP complex, the R30 loop extends over the active site, and R30 forms a salt-bridge with D73 (closed form) (Figure 5b), acting as a lid above the substrate. This was observed also in the WT-*Hs*DNPH1:dUMP complex[4] and in the E104Q-*Hs*DNPH1:5hmdUMP complex.[7] In the previously reported unliganded WT-*Hs*DNPH1, however, the R30 loop is presumably disordered, and no electron density could be seen.[4] In the current unliganded D80N-*Hs*DNPH1 subunit, the R30 loop is fully visible, furnishing insight into the conformational change that is likely required to allow substrate access to and product release from the active site (open form).

D80N-*Hs*DNPH1 makes several polar and nonpolar contacts with 5hmdUMP (Figure 5a). The nucleobase moiety is wedged between the I29 and I76 side chains. The 5′-PO_4^{2-} moiety of the substrate accepts H-bonds from the main-chain –NH of G31, R30, G100, and I29, and from the side-chain –OH of S98. Interestingly, an intramolecular H-bond is present between 5hmdUMP 5′-PO_4^{2-} and 5-CH_2OH groups. This positions the substrate in the *anti*-conformation with regards to the 2′-deoxyribosyl plane and the nucleobase O2. This is the opposite conformation to that of WT-*Hs*DNPH1-bound dUMP[4] (Figure S11).

Two additional interactions not present in the WT-*Hs*DNPH1:dUMP[4] and E104Q-*Hs*DNPH1-5hmdUMP[7] structures are identified: N80 donates an H-bond to 5hmdUMP O2, and E55 accepts an H-bond from 5hmdUMP N3. The importance of the latter to substrate catalysis is likely small, since E55Q-*Hs*DNPH1 can form the covalent intermediate. The first, however, could be mechanistically relevant. The two subunits with bound substrate have subtle differences as E104, Y24, and N80 are concerned (Figure 5c and 5d). In one subunit, the nucleotide C1′ is 3.3 Å away from the E104 –COO^-, and Y24 shares a very short H-bond with E104 –COO^- and a longer one with N80 (Figure 5c). In the other subunit, the Y24-E104 H-bond is now longer than the Y24-N80 one, which is presumably required to free up the E104 –COO^- on its way to attack on C1′, now 3.1-Å away (Figure 5d). If the scenario described above is also operational in the WT enzyme, the D80 must be protonated to donate an H-bond to 5hmdUMP O2, in line with the proposal from the pH-rate profiles.

In the D80N-*Hs*DNPH1 unliganded subunit, E104 interacts with both Y24 and E55, which now blocks substrate access to the nucleophile (Figure 5e). Either E104 or E55 must be protonated in this pose. This snapshot might represent a way for E55 to regenerate its unprotonated state for the next round of catalysis, after having abstracted a proton from a water molecule in the second half-reaction.[7] Even if operational, this step would be fast, given no $^{D2O}k_{cat}$ is observed.

The D80A-*Hs*DNPH1 unliganded structure shows an H-bond between E104 and Y24 side chains (Figure 6a). Surprisingly, in the Y24F-*Hs*DNPH1 unliganded structure, the side chains of E104 and D80 move much closer to each other (Figure 6b), indicating at least one of the side chains must be in its protonated state.

Combining our structural and functional results, a mechanistic hypothesis may be put forward for the first half-reaction that refines those recently proposed,[4, 7] and envisions roles in positioning and acid-base chemistry for Y24 and D80 (Scheme 2). Y24 shares a strong H-bond with E104. This helps align E104 for optimum nucleophilic attack on the substrate. However, to make E104 sufficiently nucleophilic, this H-bond is extended and eventually disrupted as D80 pries the Y24 –OH away from E104, allowing E104 to be esterified in the 5-phospho-2-deoxyribosyl-enzyme adduct while Y24 donates an H-bond to D80. The latter pose was captured in the E104Q-*Hs*DNPH1 covalent intermediate complex structure.[7] The H-bond between D80 and 5hmdUMP O2 may also play a role in positioning, by pulling the substrate closer to E104. Following formation of the likely anionic 5hmUra, D80 acts as a general acid to protonate it, in a step that is not rate-limiting. This interpretation explains the reduced k_{cat} for D80N-*Hs*DNPH1 (the anionic 5hmUra must be protonated by a different group not as ideally positioned to do so) and a more significantly reduced k_{cat} for D80A-*Hs*DNPH1 as even the positioning and E104 nucleophilicity-modulation roles afforded by N80 are lost. Y24 is important for proper positioning of E104 and for preventing D80 and E104 from coming in close contact with each other, which would be detrimental to nucleophilic attack, explaining the reduction in Y24F-*Hs*DNPH1 k_{cat}.

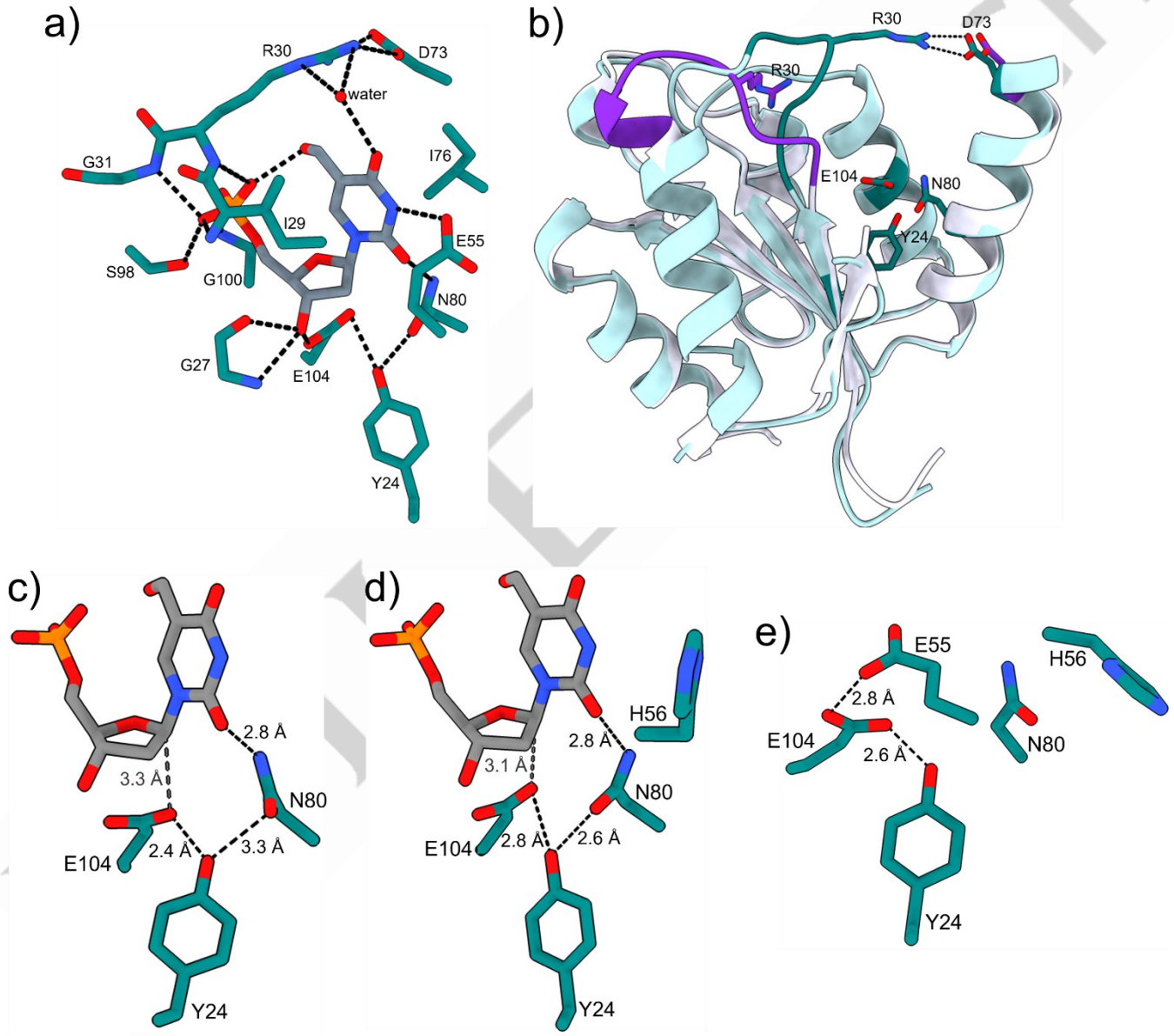

Figure 5. Crystal structures of D80N-*Hs*DNPH1. a) Active-site close-up of D80N-*Hs*DNPH1:5hmdUMP complex. b) Cartoon depiction of the overlay between unliganded (white, with R30-loop in purple) and 5hmdUMP-bound D80N-*Hs*DNPH1 (light cyan, with R30-loop in teal) subunits. The ligand is omited for clarity. c) Stick model of the D80N-*Hs*DNPH1 catalytic triad and substrate in one subunit. d) Stick model of the D80N-*Hs*DNPH1 catalytic triad and substrate in another subunit. e) Stick model of the D80N-*Hs*DNPH1 catalytic triad in the unliganded subunit. Residues are shown in teal, and 5hmdUMP in gray. The red sphere is a water molecule. Black dashed lines depict polar interactions, whereas grey dashed lines depict distances only.

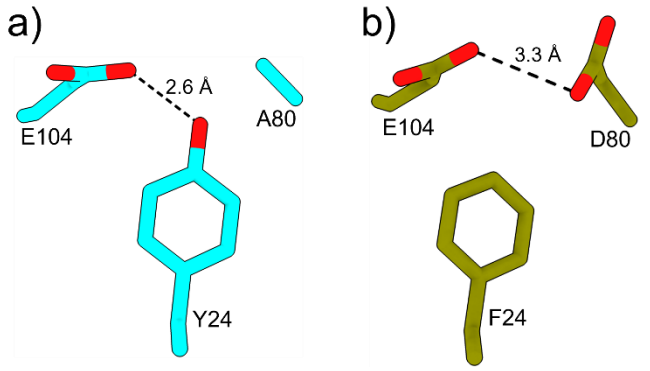

Figure 5. Crystal structures of D80A- and Y24F-*Hs*DNPH1. a) Stick model representation of D80A-*Hs*DNPH1 E104, Y24, and A80. b) Stick model representation of Y24F-*Hs*DNPH1 E104, F24, and D80. Black dashed lines represent polar interactions.

Table 1. *Hs*DNPH1 variants steady-state kinetic parameters at 25 °C and optimum pL.

*Hs*DNPH1	k_{cat} (s^{-1})	$^{D_2O}k_{cat}$[a]	k_{cat} (s^{-1}) in 9% glycerol
WT	0.22 ± 0.01	1.0 ± 0.1	0.22 ± 0.01
Y24F[b]	0.00055 ± 0.00003	1.1 ± 0.1	0.00058 ± 0.00002
D80AN[c]	0.00170 ± 0.00005	1.14 ± 0.09	0.00160 ± 0.00009
D80A[b]	0.00035 ± 0.00001	0.92 ± 0.07	0.00033 ± 0.00002
H56A[b]	0.0144 ± 0.0006	0.99 ± 0.01	0.0151 ± 0.0003
R30A[d]	0.037 ± 0.002	1.3 ± 0.1	0.040 ± 0.001

[a] Value corrected for viscosity effect. [b] pL 7.0. [c] pL 7.5. [d] pL 6.5.

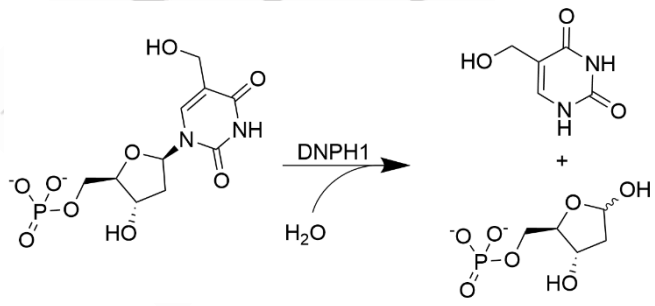

Scheme 1. Hydrolysis of 5hmdUMP catalyzed by DNPH1.

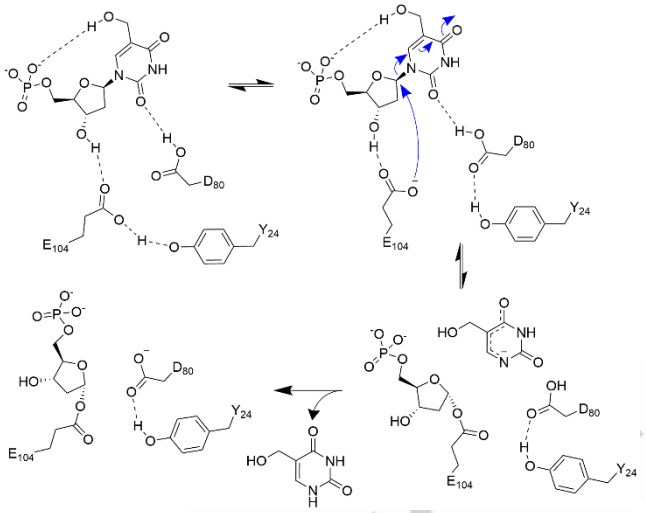

Scheme 2. Proposed mechanism for the first half-reaction of 5hmdUMP hydrolysis catalyzed by DNPH1.

Conclusion

The kinetic and site-directed mutagenesis analysis of *Hs*DNPH1, along with crystal structures of enzyme variants in unliganded and substrate-bound forms is consistent with a mechanism where proton-transfer steps do not accompany rate-limiting steps. Furthermore, D80 helps position the substrate for nucleophilic attack, and acts as the general acid for the first half-reaction, while Y24 positions E104 for catalysis. This proposal is partly related to the covalent mechanism suggested for MutY, an adenine DNA glycosylase, on the basis of quantum mechanics/molecular mechanics (QM/MM) calculations. In MutY, an asparagine is poised to position a nucleophilic aspartate for attack on the anomeric carbon.[15] Spectroscopic and QM/MM studies on *Hs*DNPH1 may uncover more details of the proposed mechanism, including evidence for the anionic 5hmdUra intermediate, charge distribution among active-site residues, and the dynamics of the R30-loop.

Experimental Section

Materials. All commercially available materials were purchased from Merck, Roche, Expedeon, Formedium, Cambridge BioScience, Agilent Technologies, Abcam, Cytiva, and ThermoFisher Scientific, and used as received unless otherwise stated. Tobacco etch virus protease (TEVP) was obtained as previously described.[16] *Escherichia coli* 5-α and BL21(DE3) competent cells were from New England Biolabs. DNA oligonucleotide primers were from Integrated DNA technologies (IDT).

Site-directed mutagenesis of *Hs*DNPH1. Expression of full-length WT-*Hs*DNPH1 for functional studies and N-terminally

truncated, otherwise WT-*Hs*DNPH1 for crystallographic studies were carried out as previously published.[4] Site-directed mutagenesis was carried out with overlapping primers according to the method of Liu and Naismith.[17] Primer sequences are listed in Table S3. For all mutants, WT-*Hs*DNPH1 expression vector[4] was used as the DNA template. The following single-amino-acid mutants were produced: Y24F-, Y24K-, Y24H-, H56A-, D80A-, D80N-, E104A, E104D-, R30A-*Hs*DNPH1. Correct insertion of each mutation was confirmed by DNA sequencing (Eurofins Genomics).

Recombinant gene expression. *E. coli* BL21(DE3) competent cells were transformed with pJexpress414 plasmids harbouring His-tagged (with a TEVP-cleavable site) *Bacillus psychrosaccharolyticus* 2'-deoxyribosyltransferase (*Bp*NDT),[9] *Drosophila melanogaster* deoxynucleotide kinase (*Dm*dNK),[10a] WT-, Y24F-, Y24K-, Y24H-, H56A-, R30A-, D80A-, D80N-, E104A, or E104D-*Hs*DNPH1. Cells were grown independently in lysogeny broth (LB) containing 100 μg mL^{-1} ampicillin at 37 °C to an optical density of 0.6 – 0.8 at 600 nm before expression was induced with 0.5 mM IPTG. Cells were grown for an additional 16 h (*Bp*NDT, *Dm*dNK) or 3 h (*Hs*DNPH1 variants) at 37 °C, harvested by centrifugation (6,774 *g*, 20 min, 4 °C), and stored at −20 °C.

Purification of *Bp*NDT and *Hs*DNPH1 variants. Each recombinant protein was purified independently, and all purification procedures were conducted on ice or at 4 ℃ using an ÄTKA Start FPLC system (GE Healthcare). All filtration of samples was by syringe through a 0.45 μm membrane. All SDS-PAGE used a NuPAGE Bis-Tris 4-12% Precast Gel (ThermoFisher Scientific) with the PageRuler Plus Stained Protein Ladder (ThermoFisher Scientific). Cells were thawed on ice and resuspended in Buffer A [50 mM HEPES, 300 mM NaCl, 10 mM imidazole, pH 7.5] containing 0.2 mg mL^{-1} lysozyme, 0.05 mg mL^{-1} BaseMuncher (Expedeon), and half a tablet of EDTA-free Complete protease inhibitor cocktail, disrupted in a cell disruptor (Constant systems) at 30 kpsi, and centrifuged (48,000 *g*, 30 min). The supernatant was filtered and loaded onto a 5-mL HisTrap FF column (Cytiva) pre-equilibrated with Buffer A. The column was washed with 20 column volumes (CV) of 10% Buffer B [50 mM HEPES, 300 mM NaCl, 500 mM imidazole, pH 7.5] and the target protein eluted with a 30-CV linear gradient of 10 – 65% Buffer B. Fractions containing the protein of interest were pooled, mixed with TEVP at a ratio of 15 mg of target protein to 1 mg of TEVP, and dialysed against 2 × 2 L Buffer C [20 mM HEPES, 150 mM NaCl, 2 mM DTT, 10% glycerol, pH 7.5], then dialysed against 2 × 2 L of Buffer A. Samples were filtered and loaded onto a 5-mL HisTrap FF column pre-equilibrated with Buffer A. The flow through was collected and analysed by SDS-PAGE. Each purified protein was dialysed against 2 × 2 L of 20 mM HEPES, 100 mM NaCl, pH 7.5. WT- and variant *Hs*DNPH1 were concentrated through a 10,000 molecular weight cutoff (MWCO) ultrafiltration membrane (Millipore). *Bp*NDT was used without further concentration. Protein concentration was determined by UV absorbance (NanoDrop) at 280 nm using theoretical molar extinction coefficients (ε_{280}) of 34,940 M^{-1} cm^{-1} (*Bp*NDT), 23,950 M^{-1} cm^{-1} (WT-*Hs*DNPH1, H56A-, D80N-, D80A-, R30A-, E104A-, E104D-*Hs*DNPH1) and 22,460 M^{-1} cm^{-1} (Y24H-, Y24F-, Y24K-*Hs*DNPH1) (ProtParam tool - Expasy). Proteins were aliquoted and stored at −80 ℃. Molecular masses of *Hs*DNPH1 variants were determined by LC-ESI/TOF-MS analysis at the University of St Andrews BSRC Proteomics and Mass Spectrometry Facility.

Purification of *Dm*dNK. Cells were thawed on ice and resuspended in Buffer A [50 mM HEPES, 500 mM NaCl, 5 mM imidazole pH 7.5] containing 0.2 mg mL^{-1} lysozyme, 0.05 mg mL^{-1} BaseMuncher (Expedeon), and half a tablet of EDTA-free Complete protease inhibitor cocktail, disrupted in a cell disruptor (Constant systems) at 30 kpsi, and centrifuged (48,000 *g*, 30 min). The supernatant was filtered and loaded onto a 5-mL HisTrap FF column (Cytiva) pre-equilibrated with Buffer A. The column was washed with 15 column volumes (CV) of 5% Buffer B [50 mM HEPES, 500 mM NaCl, 200 mM imidazole, pH 7.5], then with 15 CV of 9% Buffer B. The protein was eluted with a 20-CV linear gradient of 9 – 30% Buffer B and elution fractions analysed by SDS-PAGE. Fractions containing the protein of interest were pooled, dialysed against 2 × 2 L of 50 mM TRIS-HCl, 300 mM NaCl, pH 7.5 and concentrated. The identity of the protein was confirmed via tryptic digest and LC-MS/MS analysis of the tryptic peptides at the University of St Andrews BSRC Proteomics and Mass Spectrometry Facility.

Biocatalytic synthesis of 5hmdUMP. A reaction mixture (10 mL) of 1 mM dIMP, 1.5 mM 5-hmUra, 100 mM HEPES pH 8.0, 1 μM *Bp*NDT, and 0.3 mg of xanthine oxidase was incubated at room temperature for 3 h under gentle stirring, after which 2 μM *Dm*dNK, 5 mM $MgCl_2$, 0.375 mM ATP, 72 U/mL pyruvate kinase (Merck) and 1 mM phosphoenolpyruvate (Merck) were added, and the reaction left to proceed for a further 3 h under gentle stirring. The reaction was quenched with ice-cold methanol, vortexed and centrifuged at 3,005 *g* for 10 min to remove enzyme, and the supernatant was lyophilized. The powder was resuspended in water and loaded onto a 20-mL HiTrap Q HP anion exchange column (Cytiva) pre-equilibrated with water at 4 ℃ in an ÄTKA Start FPLC system (GE Healthcare). The column was washed with 5 CV of water, and 5hmdUMP eluted with a 30-CV linear gradient of 0 – 20% 1 M ammonium bicarbonate. Fractions exhibiting absorbance at 280 nm corresponding to 5hmdUMP were pooled, lyophilized and stored at −20 ℃. The concentration of 5hmdUMP was determined spectrophotometrically at 264 nm (ε_{264} = 10,200 M^{-1} cm^{-1})[11]. High-resolution DESI-MS, HPLC, UV-VIS spectrum, ^{31}P- and ^{1}H-NMR spectra (^{31}P- and ^{1}H-NMR were acquired on a Bruker AVIII 500 MHz in a total of 128 scans and 8 scans, respectively, with solvent lock achieved with D_2O), confirmed purity of the desired compound.

Extinction coefficient of 5-hmUra at 264 nm. The UV absorbance at 264 nm of 5-hmUra at known concentrations

(0.069 – 0.98 mM, determined spectrophotometrically at 261 nm, ε_{261} = 8,100 M^{-1} cm^{-1})[11] was measured (NanoDrop) (three independent measurements) and a standard curve of absorbance versus 5-hmUra concentration used to calculate the extinction coefficient at 264 nm.

DSF. DSF measurements (λ_{ex} = 520 ± 10 nm, λ_{em} = 558 ± 11 nm) were performed in 96-well plates on an Applied Biosystems QuantStudio™ 1 Real-Time PCR instrument. Reactions (20 µL) contained 100 mM HEPES pH 7.0 (for WT-, Y24F-, Y24H-, Y24K-, D80A-, H56A-, E104D-*Hs*DNPH1), 100 mM HEPES pH 6.5 (for R30A-*Hs*DNPH1), 100 mM HEPES pH 7.5 (for D80N-*Hs*DNPH1), 20 mM HEPES, 100 mM NaCl pH 7.5 (for E104A-*Hs*DNPH1), 8 µM enzyme and 5X Sypro Orange (Invitrogen) in the presence and absence of 30 µM 5hmdUMP. Thermal denaturation curves were recorded over a temperature range of 25 – 95 °C with increments of 0.05 °C s^{-1}. Control curves lacked protein and were subtracted from curves containing protein. All measurements were carried out in a minimum of two independent measurements.

HPLC-Based Assay of *Hs*DNPH1 Activity. Reactions (100 µL) containing 100 mM HEPES pH 7.0, 150 µM 5hmdUMP, and 20 µM either WT-, Y24F-, Y24H-, Y24K-, D80A-, D80N-, H56A-, E104A-, E104D-, R30A-, or H56A-*Hs*DNPH1 were incubated at 25 °C for 6 hours, quenched with 200 µL of ice-cold methanol, vortexed for 2 min, and centrifuged (16000 g) for 10 min. The supernatant was collected, dried under vacuum centrifugation, and resolubilized in 100 µL HPLC-grade water before 20 µL were loaded onto an Atlantis Premier BEH C18 AX column (1.7 µm, 2.1 Å~ 100 mm) on a Thermo Dionex UltiMate 3000 HPLC. The column was pre-equilibrated with 50 mM triethylamine:acetic acid pH 5.0 and run with the same mobile phase for 8 min in an isocratic manner at 0.35 mL min^{-1}. Elution was monitored by UV absorbance at 260 nm. Control lacked enzyme. Standard solutions of 1 mM 5-hmUra and 5hmdUMP were injected (10 µL) and run under the same conditions to determine 2′-deoxynucleotide and nucleobase retention time.

Spectrophotometric Assay of *Hs*DNPH1 Activity. Initial rates of enzyme-catalysed hydrolysis of 5hmdUMP at 25 °C were monitored continuously in 1-cm optical path length quartz cuvettes (Hellma) following the decrease in absorbance at 264 nm ($\Delta\varepsilon_{264}$ = 2,200 M^{-1} cm^{-1}) in a Shimadzu UV-2600 spectrophotometer outfitted with a CPS unit for temperature control. Reactions (500 µL) contained either 100 mM HEPES pH 7.0 (for WT-, Y24F-, D80A-, and H56A-*Hs*DNPH1), 100 mM HEPES pH 6.5 (for R30A-*Hs*DNPH1), or 100 mM HEPES pH 7.5 (for D80N-*Hs*DNPH1), varying concentrations of 5hmdUMP (2.5 – 20 µM for WT-*Hs*DNPH1; 30 – 70 µM for D80A- and Y24F-*Hs*DNPH1; 10 – 160 µM for R30A-*Hs*DNPH1; 2.5 – 40 µM for H56A-*Hs*DNPH1; 25 – 70 µM for D80N-*Hs*DNPH1), and one of the *Hs*DNPH1 variants. Activity of WT-*Hs*DNPH1 (0.2 – 0.4 µM) was assayed for 120 s; activity of D80A- (20 µM), Y24F- and D80N-*Hs*DNPH1 (10 µM) was assayed for 600 s; activity of R30A- and H56A-*Hs*DNPH1 (2 µM) was assayed for 180 s and 300 s respectively. Cuvettes were incubated in the spectrophotometer at 25 °C for 3 min before reaction was initiated by the addition of enzyme. Controls lacked enzyme. Two independent measurements were performed. Initial rates of WT-*Hs*DNPH1 were also measured in the presence of 20 µM 5hmdUMP and varying enzyme concentrations (0.1 – 3.2 µM).

WT- and Mutant *Hs*DNPH1 pH-Rate Profiles. The pH dependence of the reaction rate constants were determined by measuring initial rates at 25 °C via the spectrophotometric assay in a composite buffer system of 100 mM MES, 100 mM HEPES, and 100 mM TAPS pH 6.0−8.5 using the same conditions as previously described, except for 5hmdUMP concentration (2.5 – 40 µM for WT-*Hs*DNPH1; 20 – 60 µM for D80N-*Hs*DNPH1; 5 – 300 µM for R30A – *Hs*DNPH1; 2.5 – 80 µM for H56A-*Hs*DNPH1; 30 – 70 µM for D80A- and Y24F-*Hs*DNPH1). Before the pH-rate profile data were collected, enzyme stability at the extremes of the pH range used was confirmed in the following manner: each *Hs*DNPH1 variant was diluted in buffer at either pH 6.0 or 8.5 prior to the activity assay at either pH 6.5 (for R30A-*Hs*DNPH1), 7.0 (for Y24F-, D80A-, H56A-*Hs*DNPH1) or 7.5 (for D80N-*Hs*DNPH1), without any change in activity within experimental error. Two independent measurements were carried out.

***Hs*DNPH1 Activity in D_2O and Glycerol.** Initial rates of 5hmdUMP hydrolysis were measured at 25 °C in either 100 mM HEPES pH 7.0 (for WT-, Y24F-, D80A-, H56A-*Hs*DNPH1), 100 mM HEPES pH 6.5 (for R30A-*Hs*DNPH1) or 100 mM HEPES pH 7.5 (for D80N-*Hs*DNPH1) under the same conditions as described for the spectrophotometric assay, in the presence of 9% glycerol. Alternatively, initial rates of 5hmdUMP hydrolysis were measured in either 100 mM HEPES pL 7.0 (pD = pH meter reading + 0.4)[18] (for Y24F-, D80A-, H56A-*Hs*DNPH1), 100 mM HEPES pL 6.5 (for R30A-*Hs*DNPH1) or 100 mM HEPES pL 7.5 (for D80N-*Hs*DNPH1) in either 95.8% D_2O (v/v) (for D80A-), 99.4% D_2O (v/v) (for R30A-), 97.0% D_2O (v/v) (for D80N-), 97.9% D_2O (v/v) (for Y24F-), 99.3% D_2O (v/v) (for H56A-*Hs*DNPH1). For WT-*Hs*DNPH1, a pD-rate profile was built under the exact same conditions as the corresponding pH-rate profile, except it was in 99.5% D_2O (v/v). The $^{D_2O}k_{cat}$ was calculated as the ratio of the k_{cat} in H_2O to the k_{cat} in D_2O. Two independent measurements were carried out.

WT- and R30A-*Hs*DNPH1 Activity with dUMP. Initial rates of enzyme-catalysed hydrolysis of dUMP at 25 °C were monitored continuously for 10 min in 1-cm optical path length quartz cuvettes (Hellma) following the decrease in absorbance at 282 nm ($\Delta\varepsilon_{282}$ = 1,600 M^{-1} cm^{-1})[19] in a Shimadzu UV-2600 spectrophotometer outfitted with a CPS unit for temperature control. Reactions (500 µL) contained 100 mM HEPES pH 7.0, 10 µM either WT-*Hs*DNPH1 or R30A-*Hs*DNPH1 and 0 – 700 µM dUMP. The maximum dUMP concentration never exceeded 700 µM as the linear range of the spectrophotometer at 282 nm was extrapolated

at higher concentrations. Controls lacked enzymes. Cuvettes were incubated in the spectrophotometer at 25 °C for 3 min before reaction was initiated by the addition of enzyme. Two independent measurements were carried out.

Protein crystallography. N-terminally truncated Y24F-, D80A-, and D80N-*Hs*DNPH1 were purified as described for WT-*Hs*DNPH1,[4] concentrated up to 10 mg mL^{-1} in 30 mM Tris-HCl pH 7.5, 150 mM NaCl, and crystallization plates were set up with commercially available screens (Molecular Dimensions). Crystals were obtained using the sitting drop vapour diffusion method at 20 °C. Crystals of D80A-*Hs*DNPH1 were obtained in 0.1 M sodium acetate pH 4.6 and 8% PEG-4000 in 96-well plates, and cryoprotected with the same solution before flash-freezing in liquid nitrogen. Y24F-*Hs*DNPH1 crystallized in 0.2 M ammonium sulfate, 0.1 M MES, pH 6.5, 30% PEG-5000 monomethyl ether, and cryoprotected with 0.2 M ammonium sulfate, 0.1 M MES pH 6.5, 5% PEG-5000 monomethyl ether, and 30% PEG-400 before flash-freezing in liquid nitrogen. D80N-*Hs*DNPH1 crystallised in 24-well Linbro plates by mixing 2.5 μL of 10 mg mL^{-1} protein with an equal volume of reservoir buffer consisting of 25 mM sodium malonate, 37.5 mM imidazole, 37.5 mM boric acid pH 4.0, and 15% PEG-1500. Each well of the Linbro plate contained 1 mL of reservoir buffer. To obtain 5hmdUMP-bound crystals, crystals were soaked in cryoprotectant (5% PEG-1500 and 35% PEG-400 in the reservoir buffer) supplemented with 7.5 mM 5hmdUMP for 30 s before flash-freezing in liquid nitrogen. All X-ray diffraction data were collected at beamline I24 (wavelength 0.6199Å) at Diamond Light Source, UK. Unmerged MTZ was processed and scaled using the automated processing pipeline Xia2[20] integrated with DIALS[21] and further processed using AIMLESS.[22] All structures were solved by molecular replacement with PhaserMR[23] using the *Hs*DNPH1 unliganded structure (PDB ID 8OS9)[4] as the search model. Structures were refined using iterative cycles of model building with COOT[24] and refinement with either Phenix-refine[25] or Refmac.[26]

Kinetics and denaturation data analysis. Kinetics and protein denaturation data were analysed by the non-linear regression function of SigmaPlot 13.0 (SPSS Inc.). Substrate saturation curves were fitted to equation (1); bell-shaped pH-rate profiles were fitted to equation (2); thermal melting data, to equation (3); the reaction activation energies were calculated with equation (4); pH-rate profiles with pK_a either on acidic limb only or on basic limb only were fitted to either equation (5) or (6), respectively; substrate saturation curves where pseudo-first order reaction could not be assumed were fitted to equation (7); substrate-dependence of the initial rate at low subtrate concentrations was fitted to equation (8). In equations 1, 2, and 4 – 8, v is the initial rate, k_{cat} is the steady-state turnover number, K_M is the Michaelis constant, E_T is total enzyme concentration, S is the concentration of substrate, C is the pH-independent value of k_{cat}, H is the proton concentration, K_{a1} and K_{a2} are apparent acid dissociation constants, h is Planck's constant, k_B is Boltzmann constant, R is the ideal gas constant, T is the absolute temperature, $\Delta G^{\ddagger}$ is the reaction activation energy, κ is the transmission coefficient (assumed to be 1). In equation (3), F_U is fraction unfolded, T is the temperature in °C, T_m is the melting temperature, c is the slope of the transition region, and LL and UL are folded and unfolded baselines, respectively.

$$\frac{v}{E_T} = \frac{k_{cat}S}{K_M+S} \qquad \text{equation (1)}$$

$$\log k_{cat} = \log\left(\frac{C}{1+\left(\frac{H}{K_{a1}}\right)+\left(\frac{K_{a2}}{H}\right)}\right) \qquad \text{equation (2)}$$

$$F_U = LL + \frac{UL-LL}{1+e^{(Tm-T)/c}} \qquad \text{equation (3)}$$

$$k_{cat} = \kappa\frac{k_B T}{h}e^{-\Delta G^{\ddagger}/(RT)} \qquad \text{equation (4)}$$

$$\log k_{cat} = \log\left(\frac{C}{1+H/K_{a1}}\right) \qquad \text{equation (5)}$$

$$\log k_{cat} = \log\left(\frac{C}{1+K_{a2}/H}\right) \qquad \text{equation (6)}$$

$$\frac{v}{E_T} = k_{cat}\frac{E_T+S+K_M-\sqrt{(E_T+S+K_M)^2-4E_TS}}{2E_T} \qquad \text{equation (7)}$$

$$\frac{v}{E_T} = \frac{k_{cat}S}{K_M} \qquad \text{equation (8)}$$

Supporting Information

Acknowledgements

■ ACKNOWLEDGMENTS

This work was supported by the Scottish Funding Council via an IBioIC Innovation Fund grant [IBioIC 2021-01-01] to R.G.d.S. and by NuCana Plc via 50% funding of a PhD studentship to A.E.C. The authors thank the BSRC Mass Spectrometry and Proteomics Facility for protein mass analysis, and Greice M. Zickuhr for 5hmdUMP mass analysis. X-ray diffraction data were collected at Diamond Light Source (UK).

Conflict of Interests

R.G.d.S is a consultant for NuCana Plc.

Data Availability Statement

The data that support the findings of this study are available from the corresponding author upon reasonable request. Crystal structure data for D80N-, D80A- and Y24F-*Hs*DNPH1 were deposited to the PDB under IDs 8RPS, 8RPT, and 8RQD, respectively.

Keywords: DNPH1 • pH-Rate profiles • Biocatalysis • Cancer • Isotope effects

[1] Y. K. Ghiorghi, K. I. Zeller, C. V. Dang, P. A. Kaminski, *J. Biol. Chem.* **2007**, *282*, 8150-8156.
[2] K. Fugger, I. Bajrami, M. Silva Dos Santos, S. J. Young, S. Kunzelmann, G. Kelly, G. Hewitt, H. Patel, R. Goldstone, T. Carell, S. J. Boulton, J. MacRae, I. A. Taylor, S. C. West, *Science* **2021**, *372*, 156-165.
[3] H. E. Bryant, N. Schultz, H. D. Thomas, K. M. Parker, D. Flower, E. Lopez, S. Kyle, M. Meuth, N. J. Curtin, T. Helleday, *Nature* **2005**, *434*, 913-917.
[4] S. Devi, A. E. Carberry, G. M. Zickuhr, A. L. Dickson, D. J. Harrison, R. G. da Silva, *Biochemistry* **2023**, *62*, 2658-2668.
[5] C. Amiable, J. Paoletti, A. Haouz, A. Padilla, G. Labesse, P. A. Kaminski, S. Pochet, *Eur. J. Med. Chem.* **2014**, *85*, 418-437.
[6] A. G. Wagner, R. Eskandari, V. L. Schramm, *Anal. Biochem.* **2023**, *672*, 115171.
[7] N. J. Rzechorzek, S. Kunzelmann, A. G. Purkiss, M. Silva Dos Santos, J. I. MacRae, I. A. Taylor, K. Fugger, S. C. West, *Nat. Commun.* **2023**, *14*, 6809.
[8] B. Roy, A. Depaix, C. Périgaud, S. Peyrottes, *Chem. Rev.* **2016**, *116*, 7854-7897.
[9] A. Fresco-Taboada, J. Fernández-Lucas, C. Acebal, M. Arroyo, F. Ramón, I. De la Mata, J. M. Mancheño, *Catalysts,* **2018**, *8*, 8.
[10] a) B. Munch-Petersen, J. Piskur, L. Sondergaard, *J. Biol. Chem.* **1998**, *273*, 3926-3931; b) M. F. Matsuura, C. B. Winiger, R. W. Shaw, M.-J. Kim, M.-S. Kim, A. B. Daugherty, F. Chen, P. Moussatche, J. D. Moses, S. Lutz, S. A. Benner, *ACS Synth. Biol.* **2017**, *6*, 388-394.
[11] R. M. C. Dawson, D. C. Elliott, W. H. Elliott, K. M. Jones, *Data for biochemical research*, Oxford University Press, **1986**, p. 112–114.
[12] P. L. Fernandez, A. S. Murkin, *Molecules* **2020**, *25*, 1933.
[13] G. Gadda, P. Sobrado, *Biochemistry* **2018**, *57*, 3445-3453.
[14] a) R. G. Silva, M. J. Vetticatt, E. F. Merino, M. B. Cassera, V. L. Schramm, *J. Am. Chem. Soc.* **2011**, *133*, 9923-9931; b) S. S. Parikh, G. Walcher, G. D. Jones, G. Slupphaug, H. E. Krokan, G. M. Blackburn, J. A. Tainer, *Proc. Natl. Acad. Sci. USA* **2000**, *97*, 5083-5088.
[15] D. J. Nikkel, S. D. Wetmore, *J. Am. Chem. Soc.* **2023**, *145*, 13114-13125.
[16] R. Stroek, Y. Ge, P. D. Talbot, M. K. Glok, K. E. Bernas, C. M. Thomson, E. R. Gould, M. S. Alphey, H. Liu, G. J. Florence, J. H. Naismith, R. G. da Silva, *Biochemistry* **2017**, *56*, 793-803.
[17] H. Liu, J. H. Naismith, *BMC Biotechnol.* **2008**, *8*, 91.
[18] P. Salomaa, L. L. Schaleger, F. A. Long, *J. Am. Chem. Soc.* **1964**, *86*, 1-7.
[19] R. L. Miller, D. Lindstead, *Mol. Biochem. Parasitol.* **1983**, *7*, 41-51.
[20] G. Winter, *J. Appl. Crystallogr.* **2010**, *43*, 186-190.
[21] G. Winter, D. G. Waterman, J. M. Parkhurst, A. S. Brewster, R. J. Gildea, M. Gerstel, L. Fuentes-Montero, M. Vollmar, T. Michels-Clark, I. D. Young, N. K. Sauter, G. Evans, *Acta Crystallogr.. Sect. D. Struc. Biol.* **2018**, *74*, 85-97.
[22] P. R. Evans, G. N. Murshudov, , *Acta Crystallogr.. Sect. D. Biol. Crystallogr.* **2013**, *69*, 1204-1214.
[23] A. J. McCoy, R. W. Grosse-Kunstleve, P. D. Adams, M. D. Winn, L. C. Storoni, R. J. Read, *J. Appl. Crystallogr.* **2007**, *40*, 658-674.
[24] P. Emsley, K. Cowtan, *Acta Crystallogr.. Sect. D. Biol. Crystallogr.* **2004**, *60*, 2126-2132.
[25] P. V. Afonine, R. W. Grosse-Kunstleve, N. Echols, J. J. Headd, N. W. Moriarty, M. Mustyakimov, T. C. Terwilliger, A. Urzhumtsev, P. H. Zwart, P. D. Adams, *Acta Crystallogr.. Sect. D. Biol. Crystallogr.* **2012**, *68*, 352-367.
[26] G. N. Murshudov, P. Skubák, A. A. Lebedev, N. S. Pannu, R. A. Steiner, R. A. Nicholls, M. D. Winn, F. Long, A. A. Vagin, *Acta Crystallogr.. Sect. D. Biol. Crystallogr.* **2011**, *67*, 355-367.

10.1002/cbic.202400047

WILEY VCH

RESEARCH ARTICLE

Entry for the Table of Contents

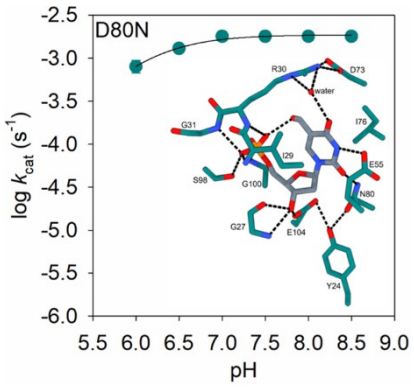

The human enzyme 2′-deoxynucleoside 5′-phosphate *N*-hydrolase 1 (*Hs*DNPH1) is a promising target for inhibition towards anticancer drug development. Crystal structures, site-directed mutagenesis, and kinetic analysis, including pH-rate profiles and solvent deuterium isotope effects, help quantify contributions from conserved residues Tyr24 and Asp80 to *Hs*DNPH1-catalysed hydrolysis of 5-hydroxymethyl-2′-deoxyuridine 5′-phosphate. These include nucleophile and substrate positioning and general-acid catalysis.